Journal of South American Earth Sciences 104 (2020) 102854

Contents lists available at ScienceDirect

Journal of South American Earth Sciences

journal homepage: www.elsevier.com/locate/jsames

# Active deformation in the San Salvador extensional stepover, El Salvador from an analysis of the April–May 2017 earthquake sequence and GPS data

D. Legrand [a,*], G. Marroquín [b], C. DeMets [c], L. Mixco [b], A. García [b], M. Villalobos [b], D. Ferrés [a], E. Gutiérrez [b], D. Escobar [b], R. Torres [b], D. Hernández [b]

[a] Universidad Nacional Autónoma de México, Instituto de Geofísica, Av. Universidad 3000, CP 04510, Ciudad de México, Mexico
[b] Observatorio de Amenazas y Recursos Naturales, Ministerio de Medio Ambiente y Recursos Naturales, Km. 5 1/2 Carretera a Santa Tecla, Colonia y Calle Las Mercedes, Plantel ISTA, San Salvador, El Salvador
[c] Department of Geoscience, University of Wisconsin-Madison, Madison, WI, 53706, USA

ARTICLE INFO

*Keywords:*
Central America
Volcanic swarm
Tectonic swarm
San salvador volcano
Bookshelf faulting

ABSTRACT

Modern and historic seismic observations indicate that earthquake swarms, often with similar characteristics, have occurred within a few tens of kilometers of the San Salvador volcano, which poses a major active hazard to the San Salvador metropolitan area. Here, we evaluate whether the April–May 2017 earthquake sequence near the San Salvador volcanic complex was tectonic or volcanic and more broadly consider the implications of up-to-date GPS observations and seismic data for earthquake and volcano hazards in the San Salvador metropolitan area. Based on magnitudes calculated for 532 earthquakes in the April–May sequence, we report a Gutenberg-Richter law b-value of 0.95 ± 0.12, consistent with b values for tectonic earthquakes, and based on temporal distribution of aftershocks we report an Omori law p-value of 1.5 ± 0.1. Focal mechanisms estimated for the mainshock and 14 largest foreshocks and aftershocks are all strike-slip with NNE-striking, left-lateral-slip and ESE-striking right-lateral-slip nodal planes. The best located foreshocks and aftershocks unequivocally indicate that the earthquake sequence accommodated left-lateral slip along a NNE-striking fault, compatible with the local tectonic setting. An absence of seismic and GPS evidence for any unrest of the San Salvador volcano during the years after the 2017 earthquake sequence is consistent with its tectonic origin. Continuous GPS measurements at a site 5 km south of the volcano reveal a previously unknown inflationary episode from mid-2010 to mid-2012, but no evidence for volcanic unrest in 2017 or later. Updated GPS velocities indicate that ~4–5 mm $yr^{-1}$ of E-W-dominated stretching occurs between the San Salvador volcano and Ilopango caldera. That the 2017 earthquakes and $M_w = 5.7$ 1986 San Salvador earthquake both accommodated left-lateral strike-slip along NNE-striking faults suggests that the GPS-measured E-W stretching is accommodated by bookshelf faulting between blocks that rotate clockwise in response to 10 ± 1.4 mm $yr^{-1}$ (95%) of dextral motion across the volcanic arc at the location of San Salvador.

## 1. Introduction

Historically, upper crustal earthquakes on faults within and near the Central America Volcanic Arc (CAVA in Fig. 1) have been responsible for ~90% of earthquake-related fatalities from Guatemala to Nicaragua, with the other ~10% attributable to earthquakes on the Middle America subduction zone (White and Harlow, 1993). The destructive potential of volcanic arc earthquakes due to their shallow depths (<15 km), proximity to cities, and frequency of occurrence (Montessus de Ballore, 1888; White, 1991) has motivated numerous studies of the seismic cycle of the volcanic arc faults (*e.g.* White, 1991; White and Harlow, 1993; Martínez-Díaz et al., 2004; Alonso-Henar et al., 2018) and the tectonic setting of the volcanic arc (e.g. Corti et al., 2005; Funk et al., 2009; Alvarado et al., 2011; Staller et al., 2016). Other authors have examined linkages and possible feedbacks between CAVA faulting, eruptions, and magmatism based on historic and recent occurrences of significant

* Corresponding author.
*E-mail addresses:* denis@geofisica.unam.mx (D. Legrand), gmarroquin@marn.gob.sv (G. Marroquín), chuck@geology.wisc.edu (C. DeMets), lmixco@marn.gob.sv (L. Mixco), rgarcia@marn.gob.sv (A. García), avillalobos@marn.gob.sv (M. Villalobos), dolomita70@gmail.com (D. Ferrés), egutierrez@marn.gob.sv (E. Gutiérrez), descobar@marn.gob.sv (D. Escobar), rtorres@marn.gob.sv (R. Torres), ahernandez@marn.gob.sv (D. Hernández).

https://doi.org/10.1016/j.jsames.2020.102854
Received 12 June 2020; Received in revised form 14 August 2020; Accepted 26 August 2020
Available online 2 September 2020

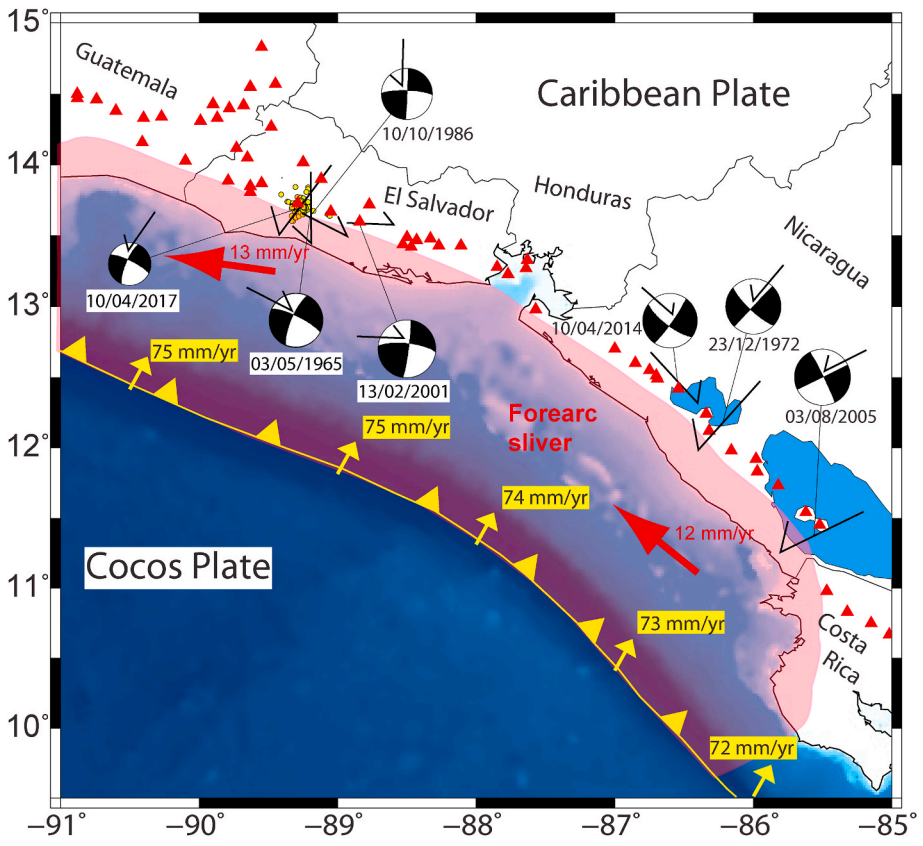


**Fig. 1.** Tectonics of the study region. Yellow arrows show velocities of the Cocos plate relative to the overlying forearc sliver (reddish shaded region), which are oriented N29°E everywhere between Guatemala and Costa Rica and decrease progressively toward the southeast from 75 to 72 mm $yr^{-1}$ (Ellis et al., 2019). Relative to the Caribbean plate, the forearc sliver moves to the northwest at rates of 12 ± 1 mm $yr^{-1}$ in Nicaragua and 13 ± 1 mm $yr^{-1}$ in El Salvador (red arrows) (Ellis et al., 2019). Red triangles locate active volcanoes in the Central American volcanic arc. Yellow circles are the earthquakes of the April-May 2017 sequence. Focal mechanisms are displayed for crustal earthquakes with known fault planes; black arrows show the slip direction on the fault plane and the corresponding slip motion along the volcanic arc. (For interpretation of the references to color in this figure legend, the reader is referred to the Web version of this article.)

earthquakes shortly before eruptions (*e.g.* Van Wyk de Vries and Merle, 1998; La Femina et al., 2004; Cailleau et al., 2007; Garibaldi et al., 2016).

In this study, we analyze local and regional seismic observations of the April-May 2017 earthquake sequence ~5–7 km southeast of the Boquerón crater of the San Salvador volcanic complex and updated GPS data in order to better understand seismic hazards and active deformation within the San Salvador extensional stepover (abbreviated SSES hereafter), where ~ E-W-directed dextral slip between the Central America forearc sliver and Chortis Block/Caribbean plate is transferred gradually northward from the San Vicente fault segment of central El Salvador to other volcanic arc faults in western El Salvador. We first consider whether the 2017 earthquake sequence was purely tectonic or was instead volcano-tectonic, and thus a possible precursor to eventual unrest of the volcano. We then use GPS measurements within and near the SSES and focal mechanisms for the 2017 and previous earthquake sequences near San Salvador to describe a tectonic framework for how CAVA faulting in the SSES accommodates the westward movement of the Central America forearc sliver (Fig. 1).

The San Salvador metropolitan area, with a 2020 population of ~2 million (Dygestic, 2014), occupies much of the earthquake-prone SSES. Historically, the city of San Salvador has been affected by numerous moderate-magnitude shallow earthquakes (Table 1), some that have caused major damage or complete destruction of the city. Extending back to 1526, 40–50 earthquakes of M~5–7 have impacted San Salvador (Table 1). The destructive $M_w$ 5.7 1986 San Salvador earthquake, which was the first to be studied with a modern seismographic network, accommodated left-lateral slip on a shallow NNE-trending fault below the city (Harlow et al., 1993). In contrast, seismic and other evidence indicates that the $M_S$~6 1965 and $M_W$6.6 2001 earthquakes both accommodated dextral slip on ~ E-W-trending faults sub-parallel to the CAVA (White et al., 1987; Martínez-Díaz et al., 2004). Distinguishing between these two (and other) possible rupture mechanisms for the 2017 earthquake sequence is an important objective of this analysis.

Five earthquakes listed in Table 1 are temporally related to volcanic activity. In September 1650, a large earthquake that severely damaged San Salvador city preceded the large eruption of El Playón (a scoria cone of the San Salvador volcanic complex), which began in November 1658 and lasted until 1671 (Lardé y Larín 1978; Ferrés et al., 2011). After the 1650 earthquake, intense seismic activity continued for years until the birth of this monogenetic volcano (Ferrés et al., 2011). Another earthquake in 1656 (or 1658?), which also severely damaged San Salvador city (Lomnitz and Schulz, 1966; White et al., 2004), may have preceded or influenced the November 1658 volcanic eruption. Several strongly felt earthquakes between December 1879 and January 1880, most notably the December 27, 1879 earthquake, preceded the last effusive eruption of the Ilopango caldera, which extruded the dacitic "Islas Quemadas" dome in the middle of the lake (Goodyear, 1880; Lomnitz and Schulz, 1966; Golombek and Carr, 1978; Richer et al., 2004). Two earthquakes closely preceded the 1917 eruption of the San Salvador volcano, a $M_s$6.4 earthquake at Armenia ~23 km southwest of the San Salvador volcano 1 h before the eruption and a $M_s$6.3 earthquake northeast of the volcano 30 min before the eruption (White et al., 1987; also see Alonso-Henar et al., 2018). The 1917 eruption included an effusive phase from a fissure on the volcano's north flank, which generated an andesitic lava flow that extended ~8 km from the vent, and explosive phases from the central Boquerón crater. The eruption evaporated the crater lake, gave rise to thick accumulations of pyroclasts around the vent forming the Boqueroncito scoria cone, and emitted an eruptive column of gas and ash less than 2 km high (Roy, 1957; Lardé y Larín 1978; Ferrés et al., 2011, 2013).

The clear association of these five earthquakes with volcanic eruptions underlines the importance of determining whether earthquake sequences are volcanic or tectonic in origin and better understanding how tectonic earthquakes may alter stresses in the upper crust that may influence the upward propagation of magmas or volatiles.

**Table 1**
List of earthquakes from 1526 that affected San Salvador metropolitan area from 1526 to 2017.

| Year | Month | Day | Magnitude | References |
|---|---|---|---|---|
| 1526 | July | 20 | | 1 |
| 1556 | ? | ? | | 1 |
| 1575 | June | 2 | | 1,2,3 |
| 1576 | it is in fact the 1575 earthquake | | | 4, 5 |
| 1581 | ? | ? | | 1 |
| 1594 | April | 21 | Ms = 6 - 7 | 1,3,4 |
| 1650 | September | 30 | | 1, 10 |
| 1656 or 1658 | ? | ? | | 1 |
| 1659 | September | 30 | | 3,5 |
| 1671 | August | 16 | | 1 |
| 1707? | ? | ? | | 1,5 |
| 1712 | December | 14 | Mi = 6.2 | 6 |
| 1719 | March | 6 | Mw = ~7+ | 1,5,7 |
| 1748 | March | 3 | Mi = 6.4 | 6 |
| 1765 | April | ? | Mi = 6.1 | 6 |
| 1776 | July | 6 | Mi = 6.8 | 1 |
| 1776 | November | 15 | Mi = 7.0 | 1 |
| 1783 | November | 29 | Mi = 5.9 | 6 |
| 1798 | February | 2 | Mi = 6.2 | 3,5,6 |
| 1831 | ? | ? | | 1 |
| 1839 | March | 22 | Mi = 6.2 | 3,5,6 |
| 1839 | October | 1 | Mi = 5.9 | 3,5,6 |
| 1847 | June | 23 | Mi = 6.3 | 6 |
| 1854 | April | 16 | Mi = 6.6 | 3,5,6,8 |
| 1854 | June | 11 | Mi = 6.2 | 3,5,6,8 |
| 1857 | November | 6 | Mi = 6.4 | 6 |
| 1860 | June | 21 | Mi = 6.1 | 6 |
| 1867 | March | 21 | Mi = 5.8 | 6 |
| 1867 | June | 30 | Mi = 7.1 | 1 |
| 1872 | December | 29 | Mi = 5.8 | 6 |
| 1873 | February | 22 | | 3,8 |
| 1873 | March | 4 | Mi = 6.4 | 3,5,6,8 |
| 1873 | March | 19 | Mic= 7.1 | 1,3 |
| 1879 | December | 27 | | 11 |
| 1879–1880 | Several between 20 December and 19 March | | | 4,5,11 |
| 1899 | March | 25 | Mi = 6.1 | 6 |
| 1917 | June | 8 | Ms = 6.4 | 3,5,6,8 |
| 1917 | June | 8 | Ms = 6.3 | 3,5,6,8 |
| 1919 | April | 28 | Mi = 6.0 | 3,5,6 |
| 1936 | December | 20 | Mi = 6.1 | 6 |
| 1965 | May | 3 | Mi = 6.0 | 3,5,6 |
| 1986 | October | 10 | Mw = 5.7 | 3,6 |
| 2001 | February | 13 | Mw = 6.6 | 9 |
| 2017 | April | 10 | Mw = 4.8 | |

| | |
|---|---|
| 1 | White et al. (2004) |
| 2 | Grases (1990) |
| 3 | Muñoz and Udíaz (2006) |
| 4 | Montessus de Ballore 1888 |
| 5 | Lomnitz and Schulz (1966) |
| 6 | Harlow et al. (1993) |
| 7 | Canora et al. (2014) |
| 8 | Ganse and Nelson (1982) |
| 9 | Canora (2011) |
| 10 | Ferrés et al. (2011) |
| 11 | Golombek and Carr (1978) |

Mi is the estimated surface wave magnitude deduced from isoseismal intensity maps.

## 2. Tectonic setting

San Salvador's geologic setting, which is dominated by intercalated fallout and pyroclastic flow deposits of the Ilopango and San Salvador volcanoes east and west of the city, amplifies the damage that can be caused by earthquakes of even moderate magnitudes (Harlow et al., 1993). The uppermost layers are deposits of 'Tierra Blanca Joven' (Vallance and Houghton, 2004; Hernández, 2004; Ferrés et al., 2013), products of the 539–540 CE major eruption of Ilopango caldera (Dull et al., 2001, 2019). Other urbanized areas of the San Salvador metropolitan area, especially south and southeast of San Salvador volcano, are built on the pyroclastic sequence of the San Salvador volcano (Boquerón), which consists mainly of fallout and pyroclastic flow and surge deposits of andesitic composition. Overall, the loosely consolidated nature of these deposits and a relatively shallow water table beneath some parts of San Salvador amplifies the destructive effects of seismic waves.

Structural observations from the SSES and central El Salvador Fault Zone and volcanic arc clearly indicate that movement of the Central America forearc sliver toward the WNW with respect to areas inland from the arc is accommodated by a combination of dextral slip across ~E-W-trending strike-slip faults that define the El Salvador Fault Zone and regions of extensional and/or bookshelf faulting within pull-apart basins that offset the volcanic arc (e.g. Alvarado et al., 2011; Garibaldi et al., 2016). Fault sets mapped in the field include (1) ~E-W-trending strike-slip faults that accommodate purely dextral movement of the Central America forearc sliver (Martínez-Díaz et al., 2004; Corti et al., 2005; Canora et al., 2014). (2) Predominant NW-SE-oriented normal faults that generally delimit the major pull-apart basins (Agostini et al., 2006). Many volcanic centers, including the San Salvador volcano, are located near these faults (Bosse et al., 1978; Carr, 1976, 1984). (3) N65°W -trending synthetic faults, where several monogenetic volcanoes are located (Meyer-Abich, 1956; Italtekna Consult, 1988; Sofield, 1998). (4) N170-180°E-trending antithetic faults such as the prominent fault on the west slope of Cerro El Picacho, which controlled the collapse of the ancient San Salvador volcano (Corti et al., 2005). These fault systems are present between San Salvador volcano and Ilopango caldera (Schmidt-Thomé, 1975; Sofield, 1998) and thus probably lie beneath the San Salvador metropolitan area.

Seismic studies confirm that earthquakes occur on all four of the structurally observed fault sets. Most earthquakes on the ~E-W-striking faults are tectonic (White, 1991; Corti et al., 2005), although some are volcano-tectonic (McNutt and Harlow, 1983; Yuan et al., 1984; Alvarado et al., 2011). The co-existence of nearly orthogonal sets of faults complicates identifying the fault plane for strike-slip earthquakes that do not rupture up to the surface.

The principal tectonic features in our study area are the Middle America subduction zone, where the oceanic Cocos plate subducts below the Central America forearc sliver (Fig. 1), the El Salvador Fault Zone and its associated stepovers, and the Central America Volcanic Arc (CAVA), which extends ~1500 km between Guatemala and Cost Rica. The rates that the Cocos plate subducts below the forearc sliver decrease slowly from 75 ± 2 mm $yr^{-1}$ offshore Guatemala to 72 ± 1 mm $yr^{-1}$ offshore Costa Rica (Ellis et al., 2019), close to the 70–77 mm $yr^{-1}$ Cocos plate convergence rates relative to the Caribbean plate (DeMets et al., 2010). The directions of Cocos plate convergence relative to the forearc sliver average a nearly uniform N29°E±2°, ~8° clockwise from the Cocos-Caribbean directions. The ~8° systematic difference in the directions of Cocos plate motions relative to the forearc sliver and Caribbean plate is attributable to 12–13 mm $yr^{-1}$ of northwest to west-northwestward movement of the Central America forearc sliver relative to the Caribbean plate (Ellis et al., 2019), consistent with an early kinematic prediction based on observed oblique subduction offshore from Nicaragua and El Salvador (DeMets, 2001).

Of direct relevance to this study, dextral shear between the forearc sliver in El Salvador and lithosphere inland from the volcanic arc is accommodated by four distinct ~ E-W-trending strike-slip faults that comprise the El Salvador Fault Zone (Martínez-Díaz et al., 2004; Corti et al., 2005; Canora et al., 2014; Alvarez-Gómez et al., 2019) and a series of pull-apart basins between these north-stepping faults. Geological and geomorphological studies of features that are offset by these four faults confirm that they accommodate horizontal dextral slip at rates of 4–11 mm $yr^{-1}$ (Corti et al., 2005; Canora et al., 2014), similar to geodetic estimates (Alvarado et al., 2011; Staller et al., 2016; Ellis et al., 2019). Within our study area, dextral slip on the San Vicente fault segment east of the Ilopango caldera is transferred to an unknown number of buried faults between the Ilopango caldera and San Salvador volcanic complex.

## 3. Seismic and GPS observations

### 3.1. Seismic data

The 2017 earthquake sequence (Figs. 1 and 2), which spanned 6 April to May 19, 2017, included 532 events that were located by the National Seismological Service of El Salvador using data from 52 local and regional broad-band and short-period seismometers and accelerometers in El Salvador, Guatemala and Nicaragua (Fig. 2a). Among these events, 70 were strong enough to be felt by people. The detection, arrival time peaking and locations were done manually, using SEISAN package (Havskov et al., 2007). The local amplitude magnitude $M_L$ of each earthquake was calculated at all the local stations for which the instrumental response was well known. The final magnitude is the average of the magnitudes at all the stations, in order to reduce the azimuthally amplitude variation due to the radiation pattern. The magnitude range (1.3–4.1 for the aftershocks) is sufficiently small not to have non-linear effects on amplitude magnitude estimation. Some of the smaller events that were recorded by fewer than three stations were located using the P-wave polarization and a distance determined from the P- versus S-wave travel time difference. As far as the errors of the locations of these earthquakes were strong, we did not take them into account in the spatial study to discriminate the fault plane, but we took them into account in the Gutenberg-Richter and Omori laws because locations are not required for these laws. Although the S–P-wave travel time difference allows us to establish these events as part of the 2017 earthquake sequence, their locations are poorly determined and we thus omit them from Fig. 2. The catalog is complete for small earthquake magnitudes, with a completeness magnitude of 1.3, which is important for our Gutenberg-Richter and Omori law analyses.

Fig. 3 shows the temporal distribution of the 532 earthquakes and their corresponding local amplitude magnitudes. The sequence can be divided into three periods (Fig. 3a), consisting of April 6–10 foreshocks prior to the April 10 mainshock (Figs. 2, 3a and 3b), and two distinct aftershock clusters (Fig. 3a and c) that were separated in time and energy release, but not in space (Fig. 2). We next discuss these in more detail.

#### 3.1.1. The April 10, 2017 mainshock

The $M_w$4.8, April 10, 2017 mainshock, which occurred at $23^h53^{mn}55s$ (UT), and had a hypocentral location of 13.702°N, 89.257°W and depth of 5.3 km as determined from the local and regional seismic data. The mainshock, which was not accompanied by any observed surface rupture, occurred 5–7 km SE of Boquerón crater of the San Salvador volcano (Fig. 2a) and had a maximum modified Mercalli intensity of V-VI (in San Salvador). The faults associated to the mainshock and aftershocks are buried due to the depth and size of the events. For example, the rupture length of the mainshock is a few kilometers (~3 km) for a $M_w$4.8 earthquake. If the square rupture starts at the middle of the fault, at about 5 km depth, the top of the subvertical fault should be at about 3.5 km depth. As far as the average dislocation on the fault is about a few centimeters, there is almost no effect that can be seen at the surface because the static displacement decays as the square of the distance which will give surface static displacement of the order of a millimeter (confirmed by the GPS CNR1 station). The aftershocks are smaller events, so it is not surprising that there are no surface ruptures associated with these events and that they (or their effects) have not been observed in previous field works. The teleseismically-derived epicentral location estimated by the U.S. Geological Survey, 13.766°N, 89.155°W, is located ~13 km northeast of our best estimate and is inconsistent with observations from our high density local and regional seismic network. Such mislocation is normal because USGS uses more distant seismic stations. Information about the mainshock focal mechanism is described in Section 4.2.

#### 3.1.2. April 6–10 foreshock sequence

A total of 77 foreshocks of magnitudes $0.8 \leq M_L \leq 4.3$ were recorded and located from April 6–10, 2017, most above depths of 6 km (Figs. 2b and 3b). The four largest foreshocks, which occurred on April 10, the day of the mainshock (Fig. 3b), consisted of a $M_L = 4.3$ earthquake 1 min before the mainshock, a $M_L = 3.6$ earthquake at $22^h21$, a $M_L = 4.0$ at $20^h02$, and a $M_L = 4.1$ earthquake at $02^h13$ (UT). All four of these similar-magnitude earthquakes were felt locally. The NS, EW, and vertical median errors of these events are 1.6 km, 1.0 km, and 1.7 km respectively (Fig. 4). The small location errors are attributable to several factors. First, data from 52 local and regional stations well distributed around the seismic sequence were used for our analysis, far more than are usually available for a local seismic study. The 52 sites include 11 stations that are located within 5 km of the seismic sequence. The data from the local stations significantly reduces the epicentral location errors because the difference time between the S and P wave arrivals generates small errors in distances and hence small errors in locations. Second the 52 stations are azimuthally well distributed with respect to the seismic sequence, with a median average gap of 130°.

The well-located earthquake aftershocks are distributed in a NNE direction and define a fault with a vertical dip (Fig. 2). Given the small uncertainties in the hypocentral locations, alternative solutions in which the aftershocks strike (for example) in the orthogonal W-WNW direction are exceedingly unlikely. We conclude with high confidence that the aftershocks accommodated sinistral slip along a NNE-striking vertical fault.

#### 3.1.3. Aftershock clusters

The aftershocks occurred into two distinct clusters based on their timing (Figs. 2 and 3a) and cumulative energy release (Fig. 3c). The first cluster spanned April 10 to 21st, immediately after the $M_W = 4.8$ April 10 mainshock. The second cluster, which extended from 23 April to 19 May, began with the relatively large $M_L = 3.7$ aftershock at $15^h51^{mn}$ (UT) on 23 April (Figs. 2, 3a and 3c). Similar to the foreshocks and mainshock, nearly all the aftershocks were located between the surface and a depth of 6 km (Fig. 2b). The two aftershock clusters lasted ~44 days, typical for a $M_w$~5 mainshock. The earthquakes on April 22, one day before the $M_L = 3.7$ April 23 earthquake, appear to be precursors of the 2nd aftershock cluster given the sudden increase in the rate of seismic energy release that occurred on April 22 (Fig. 3c). Despite these differences, the foreshocks and two aftershock clusters coincided closely in space (Fig. 2).

### 3.2. GPS data and site velocity estimation

The GPS results reported here are based on all of the GPS data that were used by Ellis et al. (2018) to derive a regional GPS velocity field for northern Central America and additional new local and regional data that have become available since that study. Within the SSES, GPS measurements began in 2001 at site SSIA ~4–5 km west of Ilopango caldera (Fig. 5). Additional campaigns and continuous GPS sites gradually densified the GPS coverage (Correa-Mora et al., 2009; Alvarado et al., 2011; Staller et al., 2016; Ellis et al., 2018, 2019). Here, we report for the first time velocities for two new continuous GPS sites PMON and SSSV (Fig. 5). Updated long-term interseismic velocities were determined for all the GPS sites in two stages. We first determined daily site positions for all the newly available GPS data using the same processing methodology as Ellis et al. (2018). We then assimilated the new and all the previously determined daily GPS site positions into a time-dependent regional elastic model that simultaneously estimates the coseismic and postseismic effects of the 2009 May 28 $M_w = 7.3$ Swan Islands, 2012 August 27 $M_w = 7.3$ Gulf of Fonseca, and 2012 November 07 $M_w = 7.4$ Champerico (Guatemala) earthquakes, and a long-term velocity at each GPS site corrected for the effects of all three earthquakes. Interested readers are referred to Ellis et al. (2018) for details about the time-dependent modelling method. Results from our GPS

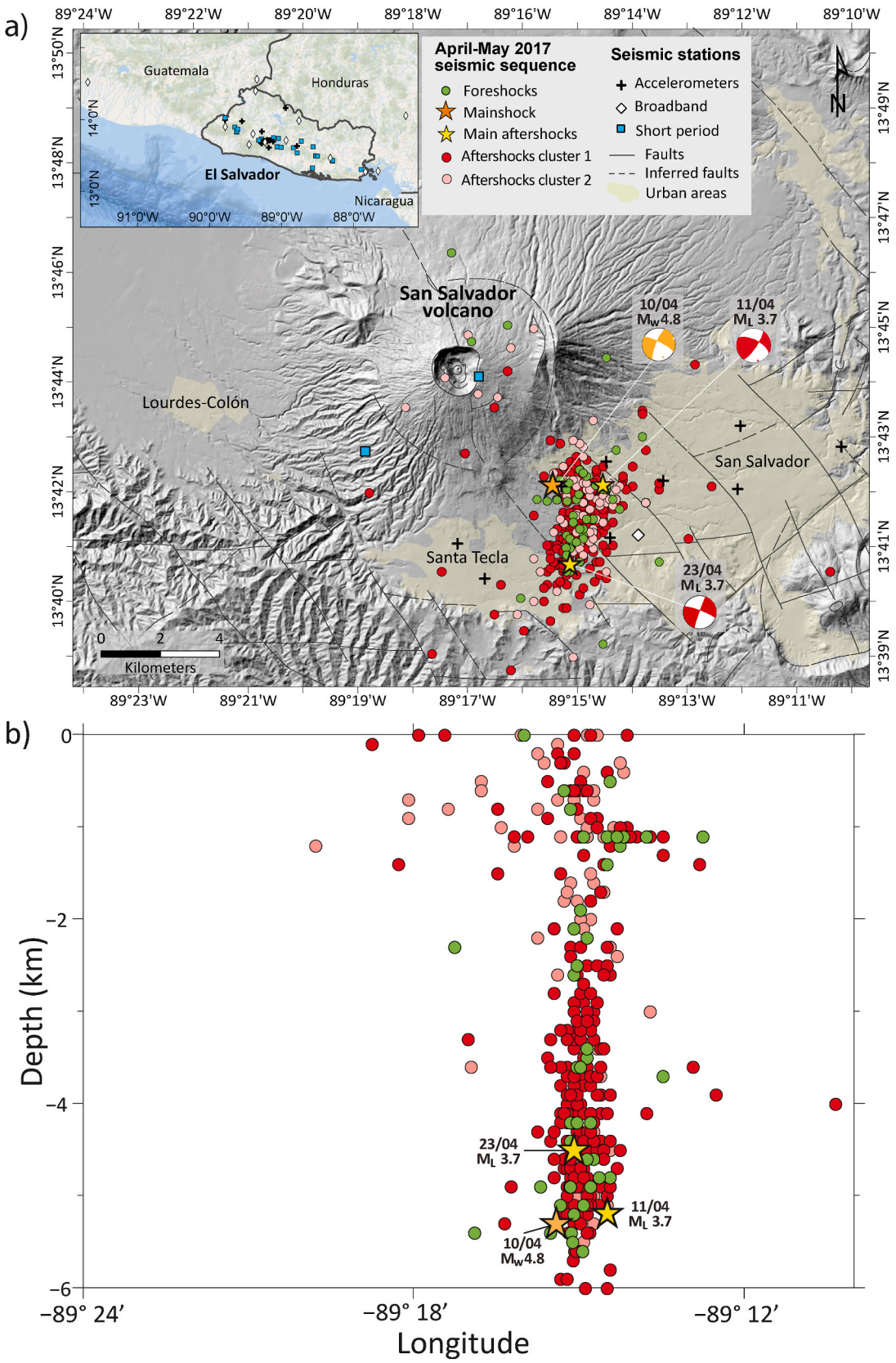


**Fig. 2.** a) Seismic stations and the 2017 earthquake locations determined with at least 4 stations. Green circles show foreshock and red (cluster 1) and pink (cluster 2) circles aftershock locations. The orange filled star with the black outline locates the mainshock ($M_W = 4.8$) on April 10, 2017 and the yellow stars with the black outline locates the largest aftershocks ($M_L = 3.7$) on 11 and 23 April. b) Depth cross section of the 6–10 April 2017 foreshock sequence. (For interpretation of the references to color in this figure legend, the reader is referred to the Web version of this article.)

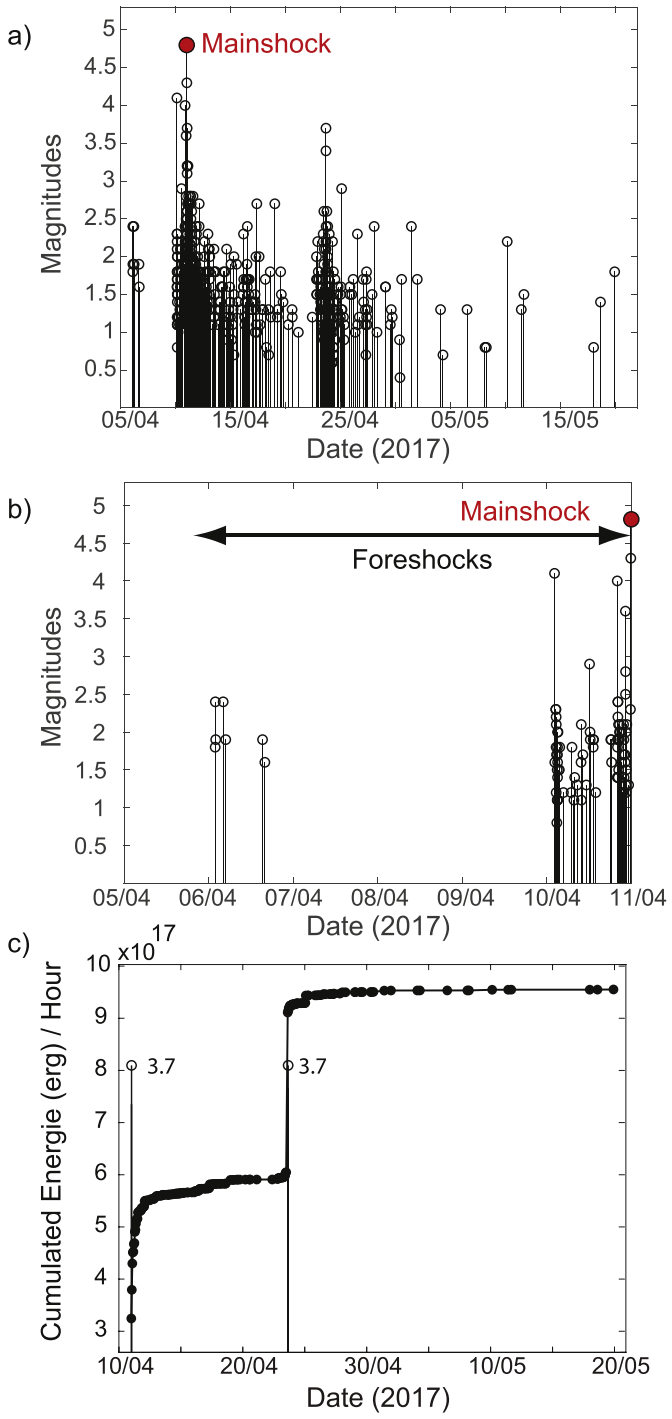


**Fig. 3.** a) Temporal distribution of the 2017 San Salvador earthquake sequence (foreshocks, mainshock, and aftershocks), spanning 6 April to 20 May. b) Earthquakes for April 6 through April 10, comprising the foreshock sequence. c) Cumulative aftershock energy release with respect to time for two distinct clusters. The magnitudes of the two largest aftershocks of 11 and 23 April (open circles) are indicated.

analysis are presented in Sections 4 and 5 and displayed in Fig. 5 and two later figures.

## 4. Results

### 4.1. The Gutenberg-Richter and Omori laws

In order to better understand the characteristics of the 2017 earthquake sequence, we first applied the Gutenberg-Richter law $\log_{10}[N(t) \geq M] = a(t) - b \cdot M$, where N(t) is the number of earthquakes larger than magnitude M during a specific time period t, a(t) is the number of earthquakes with magnitude greater than 0 during the time period, and b is a constant. We applied our analysis to all 445 aftershocks between the mainshock on April 10 and May 19, which apparently occurred on the same vertical fault (Fig. 2). We determined a single local amplitude magnitude for each earthquake by first estimating its local magnitude at each seismic station with a well-known instrumental response and then averaging the magnitudes at all the stations. Doing so reduces azimuthally dependent variations in the estimated amplitudes due to the seismic wave radiation pattern. Fig. 6 shows the cumulative and non-cumulative earthquake-magnitude distributions. The magnitude of completeness is 1.3. The distribution defines a typical Gutenberg-Richter law relationship with a b-value of 0.95 ± 0.12 and a(t) of 3.85 for the 39-day-long period from 11 April to May 19, 2017. The b-value and its 95% uncertainty were determined using the maximum likelihood method (Aki, 1965).

Although b-values have not been calculated for most previous Central America volcanic arc earthquakes due to the incompleteness of their earthquake catalogs, White et al. (1987) interpret the b-value they calculated from the 1986 San Salvador strike-slip earthquake aftershocks, 0.8 ± 0.1, as evidence that it was a purely tectonic event. The b-value we determine for the 2017 earthquake aftershocks, 0.95 ± 0.12, is also consistent with value of 1.0 commonly reported for tectonic events (Frohlich and Davis 1993), with the caveats that b values near unity have also been reported for volcano earthquake populations (Roberts et al., 2015), which is the case when no fluid is involved in non-eruptive volcanic activity and b values may be as small as 0.67 for earthquakes with surface wave magnitudes of ~5 (Okal and Romanowicz, 1994).

We next applied the Omori law ($dN(t)/dt = K/t^p$, where K and p are constants) to the two distinct aftershock clusters to find values for K and p for each (Fig. 7). For the April 10–21 aftershock cluster, the data are best fit by $p_1 = 1.5 \pm 0.1$ (Fig. 7). We excluded earthquakes that occurred on April 22, which we consider to be foreshocks to the second aftershock cluster (Section 3.1.3). The data for the April 23 (at $15^h51^{mn}$) to May 19 aftershock cluster are best fit by $p_2 = 0.9 \pm 0.1$ (Fig. 7). Any bias in our estimate of $p_2$ due to continuing aftershocks from the April 10–21 sequence is likely to be minimal given the near cessation of the cluster 1 aftershocks by April 21/22 (Fig. 3a).

### 4.2. Foreshock, mainshock, and aftershock earthquake focal mechanisms

We determined focal mechanisms for the mainshock, 4 foreshocks, and 10 aftershocks from the polarities of P-waves and via waveform modeling combined with P wave polarity analysis, with similar results. Between 20 and 45 P-wave polarities were used to determine each focal mechanism (Supplemental Material); the focal mechanisms are thus strongly constrained, with errors in our nodal plane strike, dip, and rake estimates that are unlikely to exceed a few degrees. Our best focal mechanism for the April 10 mainshock has a fault strike, dip, and rake of 203°, 75°, −13° respectively. Among the strike, dip, and rake (202°, 80°, 1°) estimates for the global centroid moment tensor (the G-CMT project, Dziewonski et al., 1981; Ekström et al., 2012), only the rake is slightly different. Our estimated focal mechanism includes a small normal component whereas the G-CMT estimate includes a small reverse component.

All 15 of our estimated focal mechanisms are consistent with either dextral strike-slip movement along a WNW-ESE-trending fault or sinistral strike-slip along a NNE-SSW-trending fault (Fig. 2a; Supplemental figure). The similarity of all the focal mechanisms is consistent with all of the earthquakes originating on the same vertical fault (Fig. 2b). In Section 5, we discuss which of the two nodal planes is the fault plane and interpret the focal mechanisms in the context of previous SSES earthquakes and our updated GPS station velocities.

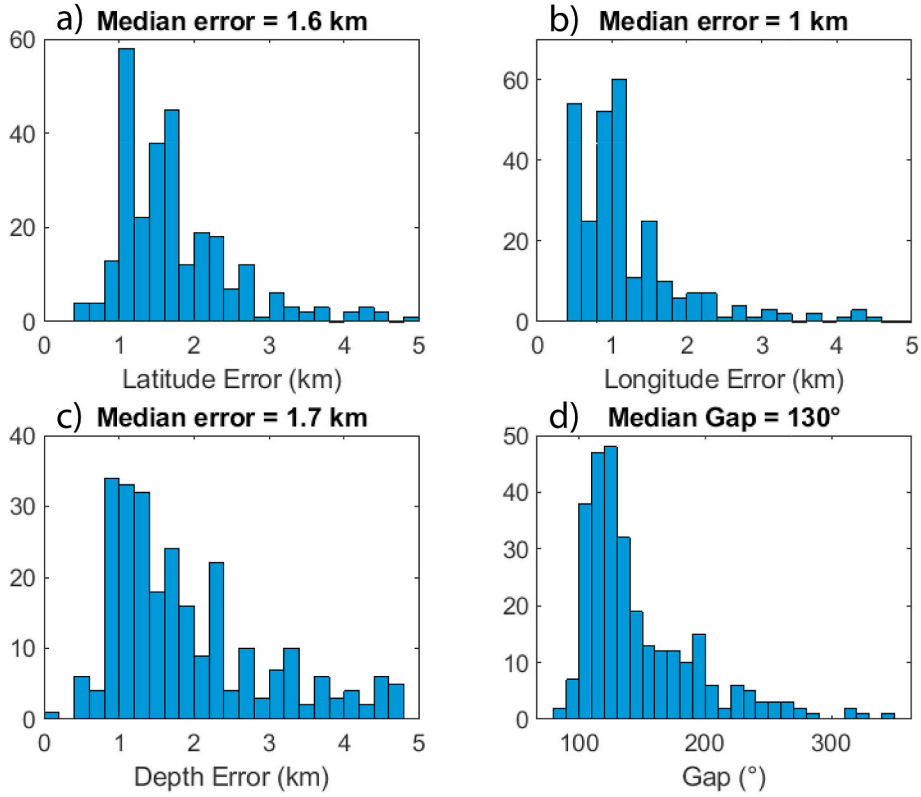


**Fig. 4.** Histograms of the location errors of earthquakes located with more or equal to 5 stations in the a) NS; b) EW, and c) vertical directions. In d) median average of the gap angle of earthquake with respect to station distribution is displayed.

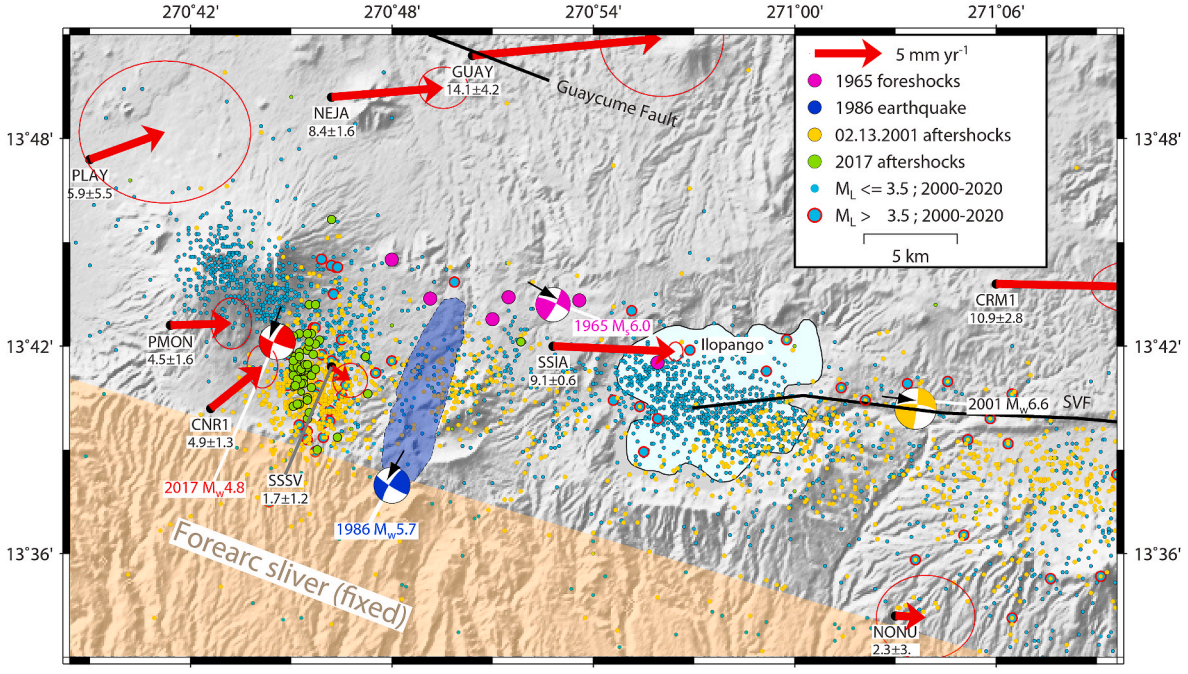


**Fig. 5.** Seismic and GPS constraints on present deformation near the San Salvador metropolitan area, which is located in Fig. 2. The GPS site velocities (red arrows) assimilate GPS data for January 2000 through 3/2020, and are corrected for the coseismic and transient postseismic effects of regional earthquakes in 2009 and 2012 (see text). The GPS site motions are shown with respect to a fixed Central America forearc sliver, whose movement is specified by the forearc sliver angular velocity of Ellis et al. (2019). The northern limit of the forearc sliver (shaded beige) is known only approximately. Each station rate and its 1-sigma uncertainty in mm $yr^{-1}$ is found beneath each 4-letter GPS site code. Earthquake epicenters are from Ministerio de Medio Ambiente y Recursos Naturales. The blue-shaded area shows the NNE-aligned aftershock zone for the October 1986 $M_w$5.7 strike-slip earthquake (blue focal mechanism). The red focal mechanism is for the April 10, 2017 mainshock (see text and Fig. 2). Foreshocks for the 1965 $M_s$6.0 earthquake are from White et al. (1987). The white or colored lines that connect each focal mechanism to its label identify the fault plane. The compressional quadrants in each focal mechanism are shaded. SVF labels the San Vicente fault segment of the El Salvador Fault Zone. (For interpretation of the references to color in this figure legend, the reader is referred to the Web version of this article.)

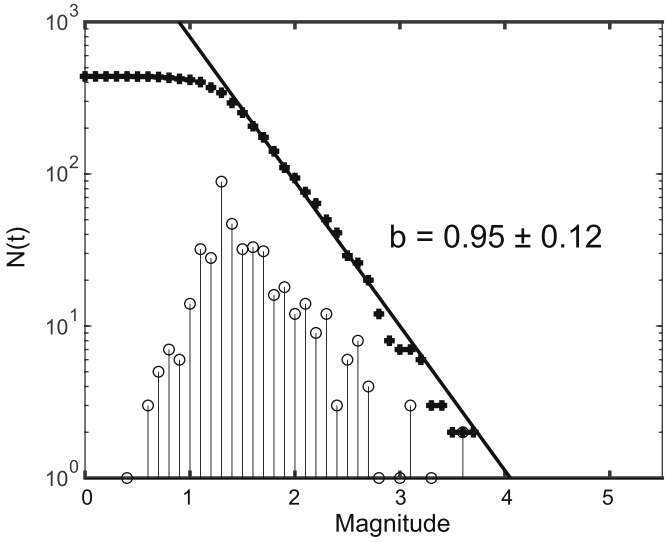


**Fig. 6.** The cumulative (black circles) and non-cumulative (open circles with stems) earthquake-magnitude distributions of the 445 aftershocks during the 39 days after the April 10, 2017 mainshock. Results from our Gutenberg-Richter law analysis (the cumulative curve) are typical of a tectonic sequence, with a b-value of 0.95 ± 0.12.

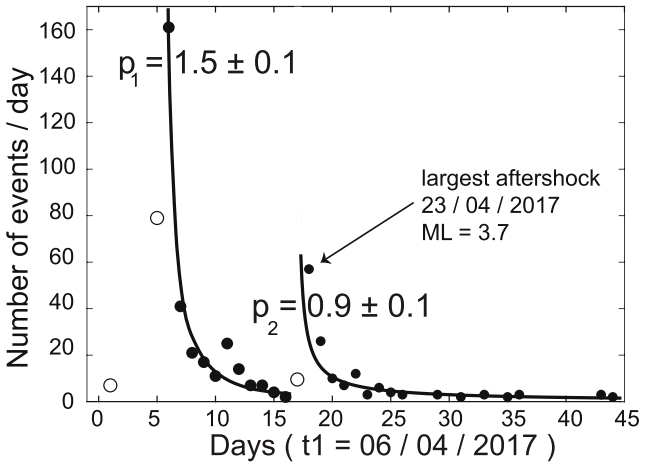


**Fig. 7.** Omori law analysis of the April 10–21 and April 23 to May 19 aftershock clusters. The foreshocks for the two aftershock clusters (white circles) were not used to estimate the p-values (see text).

### *4.3. GPS site CNR1 position time series: volcanic unrest and the 2017 coseismic offset*

GPS site CNR1, which is located ~5 km from the 2017 mainshock and San Salvador volcano (Figs. 5 and 8), is the only site close enough to record any offset due to the earthquake or determine whether the earthquake swarm occurred during a period of volcanic unrest. Below, we evaluate the full 12-year-long CNR1 time series for any evidence of transient deformation in 2017 (Fig. 8) and then examine in detail the 2017 position time series for evidence of an offset during the 2017 earthquake sequence (Fig. 9).

The highly non-linear nature of the CNR1 position time series (Fig. 8) is due partly to the coseismic and postseismic effects of three major regional earthquakes since 2009 and partly to the site's proximity to San Salvador volcano, as we discuss below. On May 28, 2009, site CNR1 moved 6 ± 1 mm toward the northeast due to the $M_w = 7.3$ Swan Islands strike-slip earthquake ~350 km northeast of CNR1 (Graham et al., 2012). The same earthquake triggered accelerated postseismic northward motion at CNR1 and elsewhere in El Salvador (Ellis et al., 2018). On August 27, 2012, CNR1 moved 6.5 ± 1 mm to the south in response to the $M_w = 7.3$ Gulf of Fonseca earthquake ~200 km south of CNR1 (Geirsson et al., 2015; Ellis et al., 2018). The same earthquake triggered transient deformation at CNR1 that is still occurring 8 years after the earthquake (Fig. 8). Finally, CNR1 moved 2 mm to the west during the November 07, 2012 $M_w = 7.4$ Champerico (Guatemala) earthquake ~350 km west of CNR1 (Ellis et al., 2018).

In the latter half of 2010, significant changes occurred in the horizontal and vertical motions at CNR1 (Fig. 8). Specifically, the slow subsidence recorded at CNR1 before mid-2010 changed to slow uplift (lower panel of Fig. 8) and the horizontal site velocity rotated by 90°, from a northwest direction before mid-2010 (blue arrow in the inset map of Fig. 8) to a southwest direction after this time (red arrow in Fig. 8 inset map). The vector difference between the velocities for the periods before and after mid-2010 (black arrow in Fig. 8 inset map) points radially outward from the San Salvador volcano.

Because the change in the 3-D station motion does not correlate with any local or regional earthquakes or with motion changes at other 8 nearby GPS sites, the cause is likely to be local to the GPS site. We interpret the onset of uplift at CNR1 and its movement away from San Salvador volcano as evidence for a previously unknown inflationary episode at San Salvador volcano that began in the latter half of 2010 and continued until at least August of 2012, when the $M_w$7.3 Gulf of Fonseca earthquake disrupted the CNR1 time series.

Fig. 9 shows daily positions for CNR1 during the months before and after the 2017 earthquake sequence. The daily site positions after the April 10 mainshock (gray circles in the pink shaded area of Fig. 9) are shifted systematically by 0.9 mm to the south and 1.1 mm to the west from positions extrapolated from the measurements for the four months before the earthquake (red lines in Fig. 9), constituting our best estimate of the horizontal coseismic offset. Estimating displacements this small is challenging due to the 1–2 mm of random noise in the daily position estimates and additional non-tectonic seasonal noise with amplitudes of up to several millimeters over time periods of months to a half-year. The CNR1 daily positions thus show that any coseismic offset from the 2017 earthquake was small (~1 mm or less in the west and south components).

In order to calculate the static ground displacement of the mainshock at CNR1 GPS station, we use a simple finite square fault and a simple circular rupture front, following Legrand and Delouis (1999). We assume a rupture area of 3 km × 3 km and that the rupture starts at the middle of the fault with a constant rupture velocity of 2.5 km/s. We also assume a 0.1s constant rise time at each point of the fault. The propagation medium is a simple half-space with Vp = 6 km/s and Vs = 3.5 km/s. We calculate the ground displacement for the two nodal planes, which don't show any significant difference on the static part of the displacement. The modeled static displacement for this simple model is ~1 mm to the south and ~1.5 mm to the west at the CNR1 station, consistent within the limitations of the data and simplified source model.

Although the consistency of the small GPS coseismic offset and the predicted elastic displacement confirms the accuracy of the focal mechanism we estimated for the main shock, the GPS site offset is insufficient to select the actual rupture plane among the two nodal planes. A comparison of the dynamic part of the seismograms of the broad band seismometers and accelerometers in our local network also failed to reveal which nodal plane is the fault plane, as is sometimes possible for larger earthquakes (Delouis and Legrand, 1999).

## 5. Discussion

San Salvador's record of recent and historic destructive earthquakes (Table 1) includes earthquakes immediately before the birth of the 1658 El Playón monogenetic volcano, before the 1879–1880 Ilopango caldera eruption and 1917 San Salvador volcano eruption (e.g. Lardé y Larín

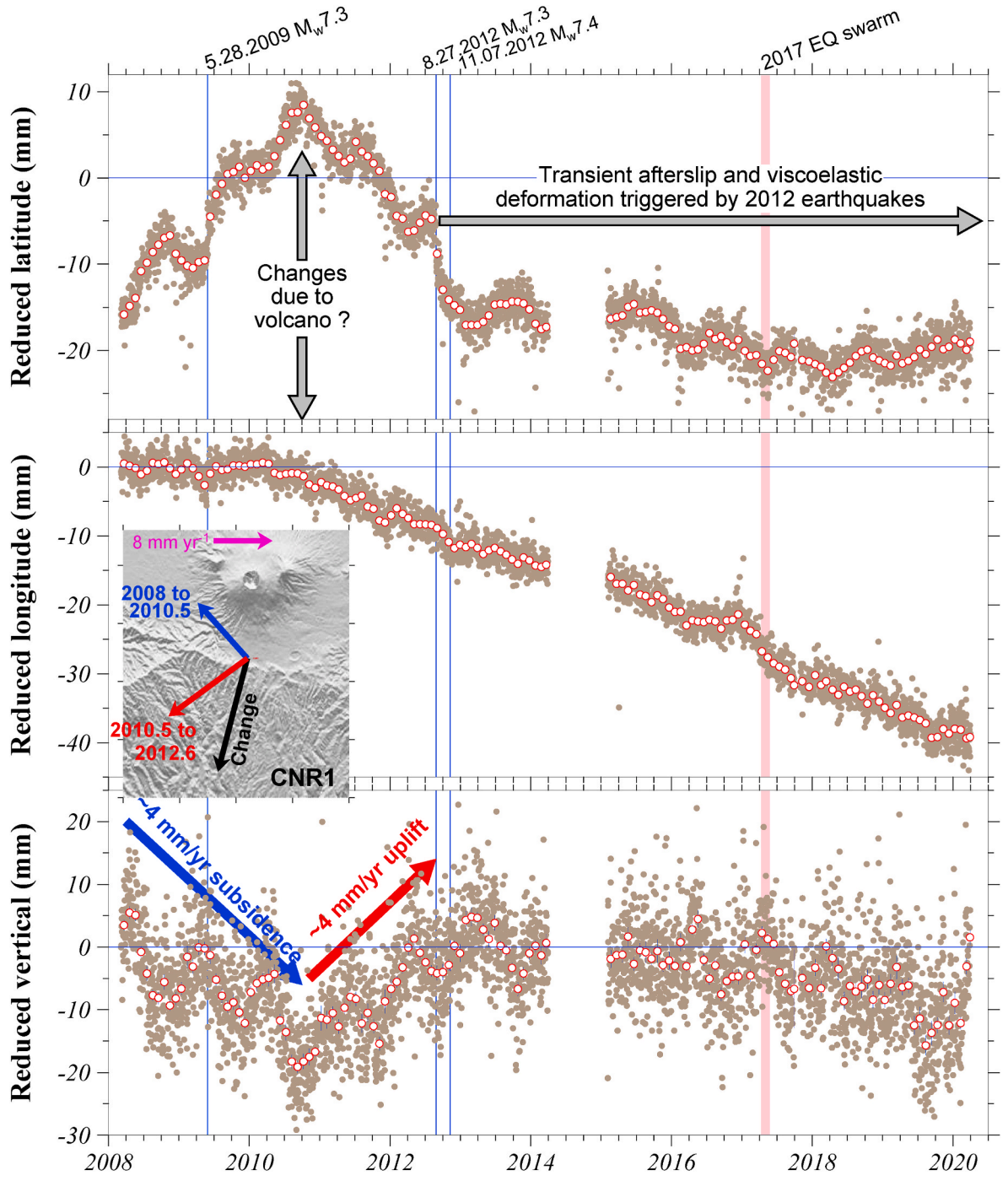


**Fig. 8.** Daily (gray circles) and monthly-average (red circles) changes in the north, east, and vertical positions of GPS site CNR1 (inset map), 2008.0 to March 2020. The horizontal lines centered at zero in the upper two panels represent respective north and east slopes of 2 and 3.6 mm $yr^{-1}$, which we selected to emphasize slope changes in the observed site locations. The change from slow subsidence to slow uplift after mid 2010 coincided with a change from NW-directed to SW-directed horizontal site motion before and after this time (blue and red arrows in inset map, respectively). The vector difference between these two velocities, shown by the black velocity arrow in the inset map, points radially outward from San Salvador volcano, consistent with slow inflation of the volcano after mid 2010. The velocities in the inset map are relative to a stationary Caribbean plate. (For interpretation of the references to color in this figure legend, the reader is referred to the Web version of this article.)

1978; Ferrés et al., 2011; Lomnitz and Schulz, 1966; White et al., 1987; Harlow et al., 1993). Below, we discuss the significance of the 2017 earthquake sequence in the context of previous seismicity in El Salvador and the nearby region of Nicaragua, after which we discuss the implications of the available seismic and geodetic constraints for deformation and hazards in the San Salvador region.

### 5.1. Origin and significance of the 2017 earthquake sequence

Three types of observations suggest that the origin of the 2017 earthquake sequence was tectonic. First, the absence of any obvious transient deformation at continuous GPS site CNR1 near San Salvador volcano before or during the 2017 earthquake sequence (Figs. 5, 8 and 9) argues against a volcanic trigger for this earthquake sequence.

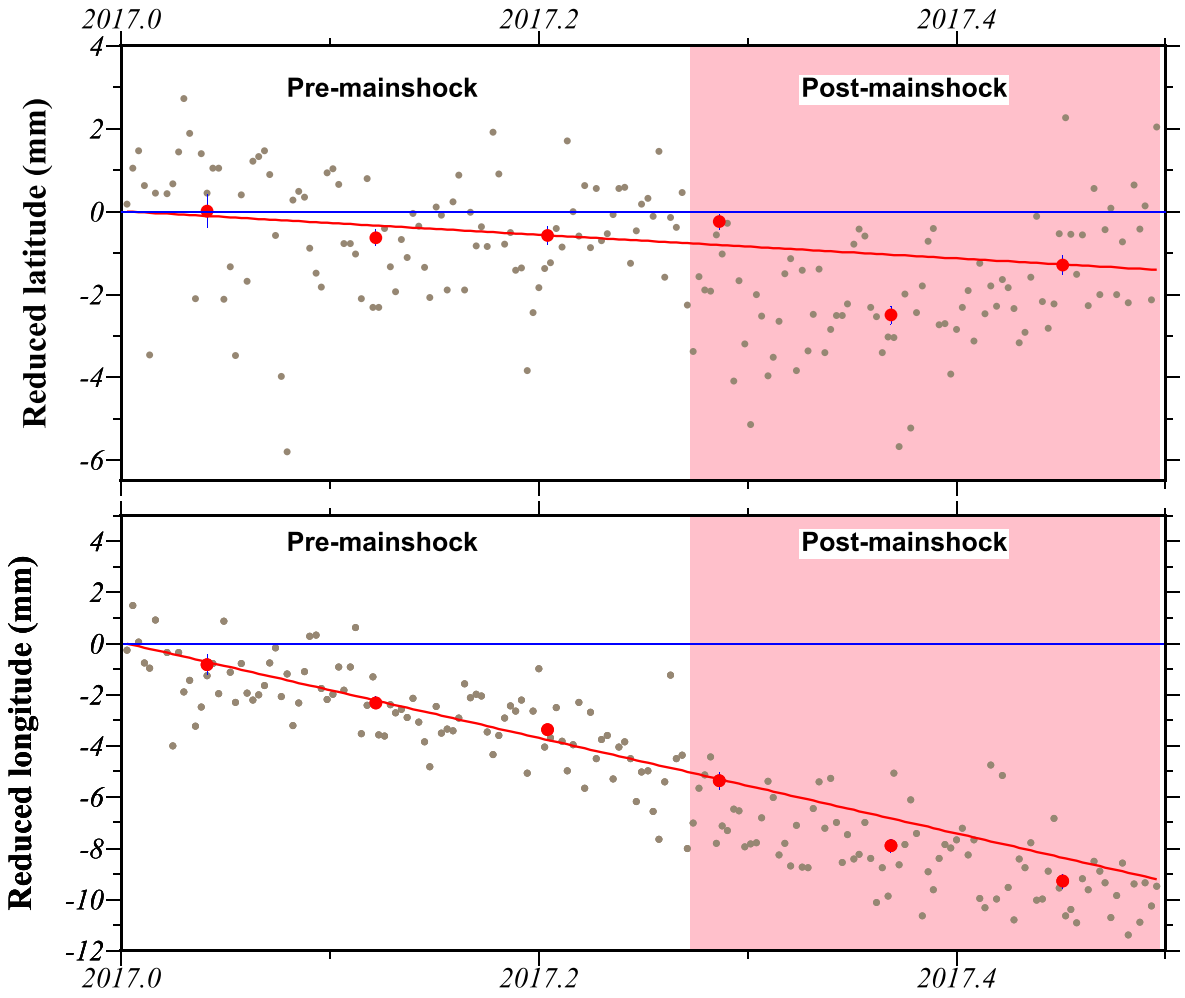


**Fig. 9.** Daily (gray circles) and monthly-average (red circles) changes in the north and east positions of GPS site CNR1 for Jan. 1 to June 30, 2017, spanning the $M_w$4.8 April 10 mainshock. Observations in the white and pink-shaded regions are from before and after April 10, respectively. The red lines, which best fit all the daily site positions before the earthquake, predict where CNR1 would be located if the April 10 earthquake had not occurred. The estimated movement of the Caribbean plate in the ITRF2014 frame of reference has been subtracted from the daily and monthly site positions in order to emphasize the small coseismic shift in the site location. (For interpretation of the references to color in this figure legend, the reader is referred to the Web version of this article.)

Second, the ~N–S alignments of the foreshocks and aftershocks (Fig. 2a) and highly consistent focal mechanisms estimated for the foreshocks, mainshock, and aftershocks (Fig. 2a; Section 4.2 and Supplemental figure) indicate that the earthquakes accommodated left-lateral slip along a NNW-striking, nearly vertical fault (Fig. 2b). Finally, the b value of 0.95 ± 0.12 for the April 10 to May 19 aftershocks differs insignificantly from unity, as expected for earthquakes with a tectonic origin (Section 4.1).

In a review of San Salvador's seismic history, Harlow et al. (1993) report that the city was severely damaged by upper crustal earthquakes at least 9 times between 1700 and 1990, not including the earthquakes in 2001 and 2017 that also impacted the metropolitan area. Of these earthquakes, reliable epicenters and focal mechanisms have been determined for the $M_s$6.0 1965 (White et al., 1987), the $M_w$5.7 1986 (White et al., 1987; Harlow et al., 1993), the $M_w$6.6 2001 (Bommer et al., 2002), and the 2017 earthquakes (all shown in Fig. 1). The 1965 earthquake, which ruptured an unexposed fault below the city, and 2001 earthquake on the San Vicente fault, east of the city, both accommodated dextral slip along ~ E-W-striking faults. In contrast, the 1986 and 2017 earthquakes both accommodated sinistral slip on buried NNE-SSW-striking faults at high angles to the arc (Fig. 5). Deformation in the SSES is therefore accommodated by opposite-sense strike-slip movement along two sets of faults that are at high angles to each other, similar to bookshelf faulting that occurs in Nicaragua (La Femina *et al.* 2002; French et al., 2010). We next discuss this in the context of the well identified fault planes of the 1986 and 2017 Salvadorian earthquakes and the 1972 and 2005 Nicaraguan earthquakes and updated GPS site velocities from this area (Fig. 5).

### 5.2. *GPS and seismic constraints on deformation in the San Salvador extensional stepover*

Relative to a stationary forearc sliver south of the volcanic arc, the GPS sites within our study area move dominantly eastward (Fig. 5), recording dextral shear between the forearc and Chortis block inland from the arc (Ellis et al., 2019). There are two significant GPS velocity gradients across the San Salvador metropolitan region, namely a ~10 mm $yr^{-1}$ south to north change in the site velocities and a ~4–5 mm $yr^{-1}$ west to east change between the San Salvador volcano and Ilopango caldera. The S-to-N velocity gradient, which samples the full movement of the forearc sliver relative to areas inland from the arc, agrees with previous GPS results (Correa-Mora et al., 2009; Alvarado et al., 2011; Staller et al., 2016; Ellis et al., 2019). The W-to-E gradient is defined by the difference between the 9.1 ± 0.6 mm $yr^{-1}$ velocity of site SSIA near the Ilopango caldera and the velocities of three GPS sites (CNR1, PMON, and PLAY) at the western limits of our study area (respectively 4.9 ± 1.3 mm $yr^{-1}$, 4.5 ± 1.6 mm $yr^{-1}$, and 5.9 ± 5.5 mm $yr^{-1}$ in Fig. 5).

The W-to-E velocity gradient (Fig. 5) indicates that E-W to ENE-WSW

stretching occurs between the San Salvador volcano and Ilopango caldera. The GPS-derived velocity gradient agrees with independent structural evidence for NE-to ENE-oriented elongation of this region from an analysis of faulting of >23,000-yr-old tephras in the Tierra Blanca sequence (Garibaldi et al., 2016). The seismic evidence described in the previous section suggests this elongation is accommodated by bookshelf faulting between clockwise-rotating blocks whose eastern and western limits are defined by NNE-striking faults at high angle to the volcanic arc (Fig. 10).

East of the Ilopango caldera, the earthquakes for the period 2000–2020 are nearly all located south of the San Vicente segment of the El Salvador fault zone (bold line in Fig. 5). Slip rates for the San Vicente segment estimated from fault trenching, river offsets, and offsets of large structures are variously 3–5.5 mm $yr^{-1}$ for the past 1 Myr (Canora et al., 2012, 2014), roughly half of the 10 ± 1.4 mm $yr^{-1}$ (95% uncertainty) full slip rate between the forearc sliver and Chortis block north of the arc (Ellis et al., 2019). The seismic and GPS evidence thus both suggest that the San Vicente fault segment is the northern limit of a 5-10-km wide zone of distributed deformation that accommodates dextral movement across the volcanic arc. West of the Ilopango caldera in the SSES, most seismicity is located south of the buried rupture zone for the $M_s$6.0 1965 earthquake and its foreshocks (violet focal mechanism and circles in Fig. 5). GPS site SSIA, which is located along the trend defined by the 1965 earthquake and its foreshocks, moves at 90% of the full rate between the forearc and Chortis block. The GPS and seismic evidence thus both suggest that the 1965 rupture zone may define the northern limit of bookshelf faulting in this area. Most deformation associated with the movement between the forearc and Chortis block thus appears to occur south of site SSIA and the 1965 rupture zone (Fig. 10).

Although our evidence suggests that most motion between the forearc and Chortis block is accommodated by deformation south of or along the 1965 earthquake rupture zone, elastic half-space modeling by Staller et al. (2016) of GPS velocities within a transect of the SSES suggests that up to 8 mm $yr^{-1}$ of dextral slip may occur along the Guaycume Fault (Fig. 5), which is located in a nearly aseismic region north of the 1965 rupture zone. Our new GPS velocities do not support a Guaycume fault slip rate this fast. Instead, the velocities of GPS sites NEJA and SSIA south of the Guaycume fault (Fig. 5) differ by only 1.8–2.5 mm $yr^{-1}$ from the velocities of two GPS sites ~10 km north of the Guaycume Fault, inconsistent with a 8 mm $yr^{-1}$ fault slip rate. By inference, most (~90%) of the dextral shear across the San Salvador step-over must occur south of sites SSIA and NEJA, as is proposed above. More GPS sites in this area are clearly needed (Section 5.4) given its importance for understanding earthquake hazards in the SSES.

### 5.3. Bookshelf faulting, earthquake triggering, and volcano-earthquake interactions

Deformation along the Nicaragua volcanic arc and in the southern Salton Trough (in southern California) has kinematic similarities to the SSES that may offer useful insights into SSES deformation characteristics such as earthquake triggering/clustering and volcano/earthquake interactions. We begin with the Nicaragua volcanic arc, where left-lateral strike-slip earthquakes on well mapped, northeast-striking faults transverse to the Nicaraguan volcanic arc include the destructive 1931 and 1972 Managua earthquakes (La Femina *et al.* 2002) and $M_w$ 6.3 2005 Lake Nicaragua earthquake (French et al., 2010), and right-lateral, strike-slip earthquakes occurred in 2014 and possibly 1955 on northwest-striking, arc-parallel faults (Suárez et al., 2016). These earthquakes are widely interpreted as evidence that bookshelf faulting accommodates dextral shear along the Nicaraguan volcanic arc (La Femina *et al.* 2002; French et al., 2010; Suárez et al., 2016).

Cailleau et al. (2007) show that dextral shearing of a 2-D finite element model in which weak volcanic centers are embedded within a strong crust predicts Coulomb failure stresses between the volcanic centers that preferentially promote the failure of arc-normal faults. Bookshelf faulting in Nicaragua may thus be a simple outcome of rheologically weak volcanic centers that are located within a dextral shear zone. Similarly, bookshelf faulting may be favored in the SSES (Fig. 10), where the Ilopango and San Salvador volcanic centers are separated by only ~20 km and dextral shear occurs at nearly the same rate as in Nicaragua (Figs. 5 and 10).

Other previously described characteristics of earthquakes in the SSES and along the Central America volcanic arc include earthquake clustering, which is the tendency for destructive volcanic arc earthquakes to cluster in time, extensive foreshock sequences, and earthquake swarms (White and Harlow, 1993). During the past century, whenever a destructive earthquake has occurred along the Central America volcanic arc following a period of relative seismic quiescence, another destructive arc earthquake has occurred within one month and 60 km of the first earthquake nearly half of the time (White and Harlow, 1993). We consider these likely examples of earthquake triggering, whereby an earthquake alters Coulomb failure stresses in a manner that promotes the immediate or near-term failure of other faults (e.g. Stein, 1999; Kilb et al., 2002).

Hence, when shallow strike-slip focal mechanisms are found in El Salvador (and Nicaragua), the mechanism is not necessarily a EW right-lateral strike-slip fault but it can also be a NNE left-lateral strike slip fault, and they must be studied individually to be sure which is the actual fault plane.

In the southern Salton Trough of southern California, dextral strike-slip movement between the Pacific and North America plates is accommodated by bookshelf faulting on cross-faults that are located between the sub-parallel San Jacinto fault and Brawley seismic zone. In this region, Hudnut et al. (1989) demonstrate that a $M_s$ 6.2 1987 strike-slip earthquake on the Elmore Ranch fault decreased the normal stresses across the orthogonal Superstition Hills fault, which ruptured in a $M_s$ 6.6 earthquake less than $12^h$ after the first event. Given the geometric and kinematic similarities between the Salton Trough and SSES, earthquakes on the arc-parallel or transverse faults in the SSES will alter Coulomb failure stresses acting on nearby faults so as to promote failure on some faults and inhibit failure along others (Alonso-Henar et al., 2018). We speculate that earthquake-triggered stress transfers between the numerous faults in the SSES are likely to be one reason for the frequency of earthquake swarms, foreshocks, and aftershocks in our study area, as was also suggested by Canora et al. (2010) for the February 13, 2001 earthquake near San Salvador.

Stress interactions between crustal faults and the Middle America subduction zone in central El Salvador also contribute to earthquake triggering in the SSES. One month after the January 13, 2001 $M_w$ 7.7 normal-faulting earthquake within the subducting Cocos plate below El Salvador, which caused positive changes in static Coulomb failure stresses along the San Vicente fault segment (Martínez-Díaz et al., 2004), the February 13, 2001 $M_w$ 6.6 strike-slip earthquake ruptured the 40-km-long San Vicente segment, killing or injuring nearly 4,000 people and damaging or destroying more than 60,000 buildings. Dynamic stress triggering may also be responsible of the presence of seismic swarms in an already stressed region (e.g. Gomberg and Johnson, 2005). Large intra-slab extensional earthquakes along this trench segment also occurred in June 1982 ($M_w$ 7.3) and possibly 1921 ($M_s$ 7.4) and 1932 ($M_s$ 7.1) (Ambraseys and Adams, 1996; White et al., 2004) and thus appear to play an important role in the seismic cycle of central El Salvador.

The frequent space-time clusters of moderate earthquakes in the San Salvador volcanic region may be due to a combination of tectonic and volcanic factors. The proximity of the San Salvador volcano to the 2017 seismic sequence suggests that magmatic loading could have altered the local stress enough to reactivate the nearby fault and trigger the associated seismicity, even if tectonic stresses dominate in the long run. A gradual increase in pore pressure possibly associated with long term magmatic intrusion can also decrease the normal stress across faults near a volcano without significantly altering the local stress field orientation.

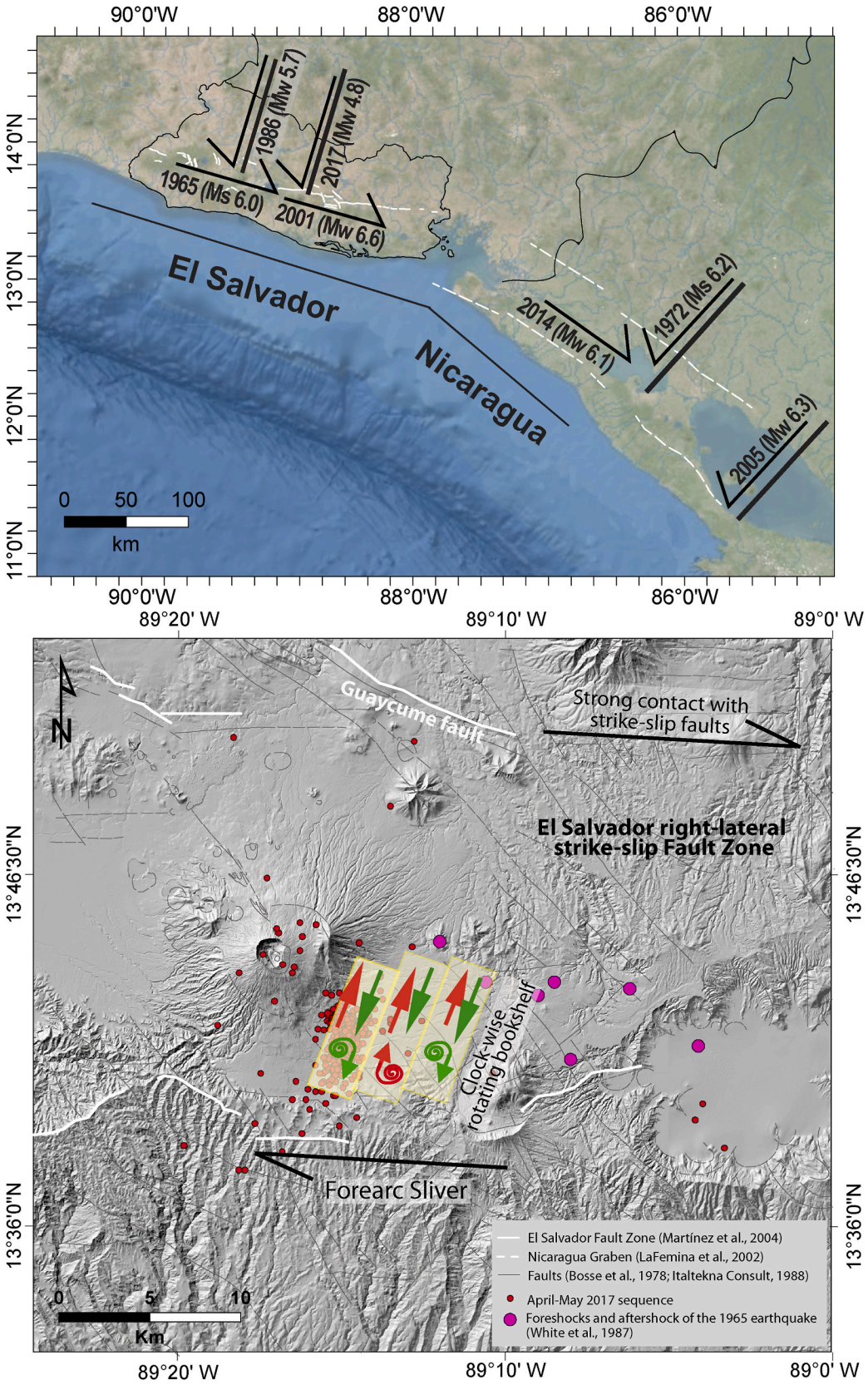


**Fig. 10.** Top) Regional context of Nicaragua and El Salvador. In white is the graben (La Femina et al., 2002) and black arrows indicate the fault planes of larger earthquakes in the region (see text). Bottom) Schematic bookshelf faulting model of the San Salvador extensional stepover. The block boundaries are approximated using the locations of the 2017 and previous earthquakes and GPS site velocities (Fig. 5). Within the uncertainties, bookshelf faulting may extend farther to the east, west and north than this depicted in the figure, but seems unlikely to extend farther southward.

Modeling of dense GPS data in El Salvador indicates that the interseismic coupling between the subducting Cocos plate and forearc sliver is weak or possibly zero (Correa-Mora et al., 2009; Ellis et al., 2019). The apparently weak coupling is consistent with evidence that only one and possibly no large-magnitude shallow-thrust subduction earthquakes have ruptured the central El Salvador trench segment since 1915 (White et al., 2004). Although the absence of large historic shallow-thrust earthquakes might indicate that El Salvador is at high risk for a future large shallow thrust earthquake (White et al., 2004), the geodetic evidence for weak coupling offshore much of El Salvador suggests that the time-integrated risk from large shallow thrust earthquakes is low. In contrast, the large intraslab and forearc earthquakes in 2001 offer clear evidence that large intra-slab extensional earthquakes and their associated triggering of shallow crustal volcanic arc earthquakes pose a significant seismic risk to El Salvador.

Finally, any evaluation of earthquake risk in the SSES must account for recent and historical associations between earthquakes and volcanic eruptions. The 1917 eruption of Boquerón, San Salvador volcano was preceded by a $M_s$ 6.4 earthquake 30–40 km west of the volcano ~1 hour before the eruption and a $M_s$ 6.3 earthquake near the volcano a half-hour before the eruption (White et al., 1987). More recently, the 1999 eruption of Cerro Negro volcano in Nicaragua was preceded by three $M_w$ ~5.2 tectonic earthquakes within a half-day and 1 km of the volcano (La Femina et al., 2004). Coulomb stress change calculations for these earthquakes indicate that they were the likely trigger for nearby earthquake swarms and the small-volume eruption outside Cerro Negro's main vent (La Femina et al., 2004). Enough historical and modern evidence thus exists to raise concerns about a possible cause-effect relationship between future earthquakes and volcanic eruptions in the SSES. This includes the San Salvador volcanic complex, which our GPS analysis indicates may have experienced an inflationary episode as recently as 2010–2012 (Fig. 8 and Section 4.3). It also includes the Ilopango caldera at the eastern limit of the San Salvador metropolitan area, whose 539/540 CE eruption had devastating local and global impacts (Dull et al., 2019) and which last erupted in 1879–1880 (Lomnitz and Schulz, 1966; Golombek and Carr, 1978). Gravity observations indicate that a fractured hydrothermal reservoir overlays a magma reservoir that extends to 6 km depth below the Ilopango caldera (Saxby et al., 2016), indicating that it still poses a major hazard.

### 5.4. *Future monitoring: A dense GPS network in San Salvador and vicinity*

More GPS sites are needed in the San Salvador metropolitan area to complement the variety of strong-motion, short-period, and broadband seismic measurements that are already made in this region. Continuous sites within 2–4 km of the San Salvador and Ilopango volcanic complexes would facilitate volcano monitoring. Campaign sites can be installed and occupied at low cost in order to reduce the inter-station spacing to ~ 1–2 km, with care taken to install stations across all faults with evidence for Quaternary activity. Three of the four continuous stations that were operating in the metropolitan area in mid-2020 (PMON, CNR1, and SSSV) are close enough to the San Salvador volcano to move measurably in response to inflationary and deflationary volcanic episodes (e.g. Fig. 8). Although the sites are separated by less than 10 km, their velocities differ substantially (Fig. 5). It is unclear whether the differences in their velocities are due to the still-short time series at sites PMON and SSSV, due to faults that may separate the three sites, or due to time-varying biases in their velocities related to activity at the nearby volcano. Observations at new continuous stations near San Salvador, but at distances farther from the volcano are needed to resolve these ambiguities.

Modeling of any velocity gradients detected by a future densified GPS network would help to constrain the long-term slip rates and interseismic coupling for active faults in the SSES. Key inputs for this modeling, namely the locations of any active faults and depths to which the faults are locked, can be determined from precisely located microearthquakes and larger events. Improvements in the accuracy of the absolute and relative locations of microseisms in the San Salvador region would thus broadly benefit efforts to fully exploit GPS data to understand faulting and earthquake hazards in this region.

## 6. Conclusions

Our analysis of the foreshocks, mainshock, and aftershocks of the 2017 earthquake sequence that occurred ~5–7 km southeast of San Salvador volcano indicates that it was a tectonic in origin and accommodated left-lateral slip on a NNE-striking vertical fault at depths between 6 km and the sub-surface. The 2008-to-present position time series for a nearby continuous GPS site shows no evidence for volcanic unrest associated with the 2017 earthquake swarm but reveals a previously unrecognized ~2-yr-long period of volcano inflation that began in the latter half of 2010. The occurrence of left-lateral strike-slip earthquakes in 1986 and 2017 on NNE-trending faults below San Salvador and likely right-lateral slip on an arc-parallel, WNW-trending fault during the 1965 earthquake indicates that bookshelf faulting occurs within the San Salvador extensional stepover. Regional GPS modeling indicates that $10 \pm 1.4$ mm $yr^{-1}$ of WNW-ESE dextral slip occurs across the San Salvador extensional stepover. We interpret earthquake locations since 2000 and our updated GPS velocities as evidence that most (90%) of the dextral shear is accommodated by deformation that occurs south of and including the 1965 earthquake rupture zone, contrary to a previous interpretation that most of the deformation occurs farther north. Our updated GPS velocities also indicate that 4–5 mm $yr^{-1}$ of extension occurs between the San Salvador volcano and Ilopango caldera. Denser GPS observations are needed to determine the locations and slip rates of the faults that accommodate this extension and the dextral shear across the volcanic arc.

## Declaration of competing interest

The authors declare that they have no known competing financial interests or personal relationships that could have appeared to influence the work reported in this paper.

## Acknowledgments

This work was supported by Panamerican Institute of Geography and History (IPGH Instituto Panamericano de Geografía e Historia), through the project GEOF03 2019 of the 2019 Projects Call, between El Salvador and México. Funding from U.S. National Science Foundation grant EAR-1144418 supported the GPS data collection and analysis. We thank three anonymous reviewers for constructive comments and contribute to improve the text.

## Appendix A. Supplementary data

Supplementary data to this article can be found online at https://doi.org/10.1016/j.jsames.2020.102854.

## References

Agostini, S., Corti, G., Doglioni, C., Carminati, E., Innocenti, F., Tonarini, S., Manetti, P., Di Vincenzo, G., Montanari, D., 2006. Tectonic and magmatic evolution of the active volcanic front in El Salvador: insight into the Berlin and Ahuachapan geothermal areas. Geothermics 35, 368–408. https://doi.org/10.1016/j.geothermics.2006.05.003.

Aki, K., 1965. Maximum likelihood estimate of bin the formula logN=a−bm and its confidence limits. Bull. Earthquake Res. Inst., Tokyo Univ. 43, 237–238.

Alonso-Henar, J., Benito, B., Staller, A., Alvarez-Gomez, J.A., Martinez-Diaz, J.J., Canora, C., 2018. Large-magnitude crustal seismic sources in El Salvador and deterministic hazard scenarios. Eng. Geol. 243, 70–83.

Alvarado, D., et al., 2011. Forearc motion and deformation between El Salvador and Nicaragua: GPS, seismic, structural, and paleomagnetic observations. Lithosphere 3, 3–21.

Alvarez-Gómez, J., Staller-Vázquez, A., Martínez-Díaz, J., Canora, C., Alonso-Henar, J., Insua-Arévalo, J., Béjar-Pizarro, M., 2019. Push-pull driving of the Central America Forearc in the context of the Cocos-Caribbean-North America triple junction. Sci. Rep. https://doi.org/10.1038/s41598-019-47617-3.
Ambraseys, N.N., Adams, R.D., 1996. Large-magnitude central American earthquakes, 1898-1994. Geophys. J. Int. 127, 665–692.
Bommer, J.J., et al., 2002. The El Salvador earthquakes of January and February 2001: context, characteristics and implications for seismic risk. Soil Dynam. Earthq. Eng. 22, 389–418.
Bosse, H., Lorenz, W., Merino, A., Mihm, A., Rode, K., Schmidt-Thomé, M., Wiesemann, G., Weber, H., 1978. Geological map of El Salvador republic: hannover Germany. In: Bundesanstalt für Geowissenschaften und Rohstoffe, (D-3 scale 1: 100,000).
Cailleau, B., LaFemina, P., Dixon, T., 2007. Stress accumulation between volcanoes: an explanation for intra-arc earthquakes in Nicaragua? Geophys. J. Int. 169, 1132–1138.
Canora, C., 2011. Análisis sismotectónico, neotectónico y paleosísmico de la zona de falla de El Salvador, Centro América. Ph.D. thesis. Geodynamics Department, Universidad Complutense de Madrid, Spain, p. 192.
Canora, C., Martínez-Díaz, J., Villamor, P., Berryman, K., Álvarez-Gómez, J., Pullinger, C., Capote, R., 2010. Geological and seismological analysis of the 13 february 2001 Mw 6.6 El Salvador earthquake: evidence for surface rupture and implications for seismic hazard. Bull. Seismol. Soc. Am. 100, 2873–2890.
Canora, C., Villamor, P., Martinez-Diaz, J., Berryman, K., Alvarez-Gomez, J., Capote, R., Hernandez, W., 2012. Paleoseismic analysis of the san Vicente segment of the El Salvador fault zone, El Salvador, Central America. Geol. Acta 10, 103–123.
Canora, C., Martinez-Diaz, J., Villamor, P., Staller, A., Berryman, K., Alvarez-Gomez, J., Capote, R., Diaz, M., 2014. Structural evolution of the El Salvador Fault Zone: an evolving fault system within a volcanic arc. J. Iber. Geol. 40, 471–488.
Carr, M., 1976. Underthrusting and quaternary faulting in northern Central America. Geol. Soc. Am. Bull. 87, 825–829.
Carr, M., 1984. Symmetrical and segmented variation of physical and geochemical characteristics of the Central American Volcanic Front. J. Volcanol. Geoth. Res. 20, 231–252.
Correa-Mora, F., DeMets, C., Alvarado, D., Turner, H., Mattioli, G., Hernandez, D., Pullinger, C., Rodriguez, M., Tenorio, C., 2009. GPS-derived coupling estimates for the Central America subduction zone and volcanic arc faults: El Salvador, Honduras, and Nicaragua. Geophys. J. Int. 179, 1279–1291.
Corti, G., Carminati, E., Mazzarini, F., Garcia, M., 2005. Active strike-slip faulting in El Salvador, Central America. Geology 33, 989–992. https://doi.org/10.1130/G21992.1.
Delouis, B., Legrand, D., 1999. Focal mechanism determination and identification of the actual fault plane of earthquakes using only one or two near source seismic recordings. Bull. Seismol. Soc. Am. 89, 1558–1574.
DeMets, C., 2001. A new estimate for present-day Cocos-Caribbean plate motion: implications for slip along the Central American volcanic arc. Geophys. Res. Lett. 28, 4043–4046. https://doi.org/10.1029/2001GL013518.
DeMets, C., Gordon, R., Argus, D., 2010. Geologically current plate motions. Geophys. J. Int. 181, 1–80.
Dull, R., Southon, J., Sheets, P., 2001. Volcanism, ecology, and culture: a reassessment of the Volcán Ilopango TBJ eruption in the southern Maya real. Lat. Am. Antiq. 12, 25–44. https://doi.org/10.2307/971755.
Dull, R., et al., 2019. Radiocarbon and geologic evidence reveal Ilopango volcano as source of the colossal 'mystery' eruption of 539/40 CE. Quat. Sci. Rev. 222, 105855.
Dygestic, 2014. EL Salvador: Estimaciones y Proyecciones de Población Municipal 2005-2025. Dirección General de Estadística y Censos (Dygestic) del Ministerio de Economía (El Salvador); Fondo de población de las Naciones Unidas (UNFPA) y Centro Latinoamericano y Caribeño de Demografía (CELADE). San Salvador, El Salvador, p. 136.
Dziewonski, A., Chou, T., Woodhouse, J., 1981. Determination of earthquake source parameters from waveform data for studies of global and regional seismicity. J. Geophys. Res. 86, 2825–2852.
Ekström, G., Nettles, M., Dziewonski, A., 2012. The global CMT project 2004-2010: centroid-moment tensors for 13,017 earthquakes. Phys. Earth Planet. In. 200–201, 1–9.
Ellis, A., et al., 2018. GPS constraints on deformation in northern Central America from 1999 to 2017, Part 1 - time-dependent modelling of large regional earthquakes and their post-seismic effects. Geophys. J. Int. 214, 2177–2194.
Ellis, A., et al., 2019. GPS constraints on deformation in northern Central America from 1999 to 2017, Part 2: block rotations and fault slip rates, fault locking, and distributed deformation. Geophys. J. Int. 218, 729–754.
Ferrés, D., Delgado Granados, H., Hernández, W., Pullinger, C., Chávez, H., Castillo-Taracena, C.R., Cañas Dinarte, C., 2011. Three thousand years of fl ank and central vent eruptions of the San Salvador volcanic complex (El Salvador) and their effects on El Cambio archaeological site:a review based on tephrostratigraphy. Bull. Volcanol. 73 (7), 833–850. https://doi.org/10.1007/s00445-011-0465-0.
Ferrés, D., Delgado-Granados, H., Gutiérrez, R., Farraz, I., Hernández, E., Pullinger, C., Escobar, C., 2013. Explosive volcanic history and hazard zonation maps of Boquerón volcano (San Salvador volcanic complex, El Salvador). In: Rose, W.I., Palma, J.L., Delgado Granados, H., Varley, N. (Eds.), Understanding Open-Vent Volcanism and Related Hazards, vol. 498. Geological Society of America Special Paper, pp. 201–230. https://doi.org/10.1130/2013.2498(12.
French, S., Warren, L., Fischer, K., Abers, G., Strauch, W., Protti, J., Gonzalez, V., 2010. Constraints on upper plate deformation in the Nicaraguan subduction zone from earthquake relocation and directivity analysis. G-eochem. Geophys. Geosyst. 11, Q03S20.
Frohlich, C., Davis, S., 1993. Teleseismic b values; or, much ado about 1.0. J. Geophys. Res. 93, 631–644.
Funk, J., Mann, P., McIntosh, K., Stephens, J., 2009. Cenozoic tectonics of the Nicaraguan depression, Nicaragua, and Median Trough, El Salvador, based on seismic-reflection profiling and remote-sensing data. Geol. Soc. Am. Bull. 121, 1491–1521. https://doi.org/10.1130/B26428.1.
Ganse, R., Nelson, J., 1982. Catalog of significant earthquakes 2000 B.C. to 1979, including quantitative casualties and damage-. Bull. Seismol. Soc. Am. 72, 873–877.
Garibaldi, N., Tikoff, B., Hernandez, W., 2016. Neotectonic deformation within an extensional stepover in El Salvador magmatic arc, Central America: implication for the interaction of arc magmatism and deformation. Tectonophysics 693, 327–339.
Geirsson, H., LaFemina, P., DeMets, C., Hernandez, D., Mattioli, G., Rogers, R., Rodriguez, M., Marroquin, G., Tenorio, V., 2015. The 2012 August 27 $M_w$7.3 El Salvador earthquake: expression of weak coupling on the Middle America subduction zone. Geophys. J. Int. 202, 1677–1689.
Golombek, M., Carr, M., 1978. Tidal triggering of seismic and volcanic phenomena during the 1879–1880 eruption of Islas Quemadas volcano in El Salvador, Central America. J. Volcanol. Geoth. Res. 3, 299–307.
Gomberg, J., Johnson, P., 2005. Dynamic triggering of earthquakes. Nature 437, 830.
Goodyear, W.A., 1880. Earthquake and volcanic phenomena: december 1879 and january 1880. In: The Republic of El Salvador. Central America. Star & Herald Office, Panamá, p. 56.
Graham, S., DeMets, C., DeShon, H., Rogers, R., Rodriguez, M., Strauch, W., Wiese, K., 2012. GPS and seismic constraints on the M=7.3 2009 Swan Islands earthquake: implications for stress changes along the Motagua fault and other nearby faults. Geophys. J. Int. 190, 1625–1639.
Grases, J., 1990. Terremotos destructores del Caribe 1502–1990. UNESCO-RELACIS, Montevideo, Uruguay, p. 132.
Harlow, D., White, R., Rymer, M., Alvarez, S., 1993. The San Salvador earthquake of 10 October 1986 and its historical context. Bull. Seismol. Soc. Am. 83, 1143–1154.
Havskov, J., Ottemoller, L., Canabrava, R., 2007. SEISAN: multiplatform implementation of MINISEED/SEED. Orpheus Newsletters 7.
Hernández, W., 2004. Geotechnical and Volcanological Characteristics of the Tierra Blanca Joven Deposits, Ilopango Caldera, El Salvador [Master of Geological Technologies Thesis]: San Salvador, El Salvador. Universidad Politécnica de Madrid, Spain, p. 117. Universidad Politécnica de El Salvador, and Madrid, Spain (in Spanish).
Hudnut, K., Seeber, L., Pacheco, J., 1989. Cross-fault triggering in the November 1987 Superstition Hills earthquake sequence, southern California. Geophys. Res. Lett. 16, 199–202.
Consult, Italtekna, Salvador, Consorzio, Mission, Italian, 1988. San Salvador, Programa di Ricostruzione: Informe Vulcanológico: San Salvador, El Salvador, Direzione Generale per la Cooperazione allo Sviluppo, Repubblica Italiana. Dirección General del Servicio Nacional de Estudios Territoriales, p. 88.
Kilb, D., Gomberg, J., Bodin, P., 2002. Aftershock triggering by complete Coulomb stress changes. J. Geophys. Res. 107 https://doi.org/10.1029/2001JB000202.
La Femina, P., Dixon, T., Strauch, W., 2002. Bookshelf faulting in Nicaragua. Geology 30, 751–754.
La Femina, P., Connor, C., Hill, B., Strauch, W., Saballos, J., 2004. Magma-tectonic interactions in Nicaragua: the 1999 seismic swarm and eruption of Cerro Negro volcano. J. Volcanol. Geoth. Res. 137, 187–199.
Lardé, y, Larín, J., 1978. El Salvador: inundaciones e incendios, erupciones y terremotos. Biblioteca de Historia Salvadoreña. Concultura, San Salvador 5, 99–134.
Legrand, D., Delouis, B., 1999. Determination of the fault plane using a single near field seismic station with a finite dimension source model. Geophys. J. Int. 138, 801–808.
Lomnitz, C., Schulz, R., 1966. The san salvador earthquake of may 3, 1965. Bull. Seismol. Soc. Am. 56, 561–575.
Martínez-Díaz, J., Alvarez-Gomez, J., Benito, B., Hernandez, D., 2004. Triggering of destructive earthquakes in El Salvador. Geology 32, 65–68. https://doi.org/10.1130/G20089.1.
McNutt, S., Harlow, D., 1983. Seismicity at Fuego, Izalco, and San Cristobal Volcanoes, vols. 46–3. Central America, pp. 283–297, 1973-1974: Bulletin Volcanologique.
Meyer-Abich, H., 1956. Los volcanes activos de Guatemala y El Salvador: anales del Servicio Geológico Nacional. El Salvador 3, 66–72.
Montessus de Ballore, F., 1888. Tremblements de Terre et éruptions volcaniques au Centre- Amerique. Dijon, Societé de Sciences naturelles de Saone-et-Loire, p. 293.
Muñoz, D., Udíaz, A., 2006. The earthquake of San Salvador, Central America, of 21 April 1594: the first questionnaires on the damage of an earthquake in the Western Hemisphere. Bull. Seismol. Soc. Am. 96, 1538–1544.
Okal, E., Romanowicz, B., 1994. On the variation of b-values with earthquake size. Phys. Earth Planet. In. 87, 55–76.
Richer, M., Mann, C., Stix, J., 2004. Mafic magma injection triggers eruption at Ilopango Caldera, El Salvador, Central America. In: Rose, W.I., Bommer, J.J., López, D.L., Carr, M.J., Major, J.J. (Eds.), Natural Hazards in El Salvador: Boulder, Colorado, vol. 375. Geological Society of America Special Paper, pp. 175–189.
Roberts, N., Bell, A.F., Main, I.G., 2015. Are volcano seismic b-values high, and if so when? J. Volc. And Geothermal Res. 308 https://doi.org/10.1016/j.volgeores.2015.10.021.
Roy, S.K., 1957. Restudy of the 1917 eruption of volcán Boquerón, El Salvador, Central America. Fieldiana-Geology Chicago Natural History Museum 10, 363–382.
Saxby, J., Gottsmann, J., Cashman, K., Gutierrez, E., 2016. Magma storage in a strike-slip caldera. Nat. Commun. 7, 12295. https://doi.org/10.1038/ncomms12295.
Schmidt-Thomé, M., 1975. The Geology in the San Salvador Area, a basis for city development and planning. Geol. Jahrb. 13, 207–228.
Sofield, D., 1998. History and Hazards of San Salvador Volcano, El Salvador [M.S. Thesis]: Houghton. Michigan Technological University, Michigan, p. 103.

Staller, A., Martinez-Diaz, J., Benito, B., Alonso-Henar, J., Hernandez, D., Hernandez-Rey, R., Diaz, M., 2016. Present-day crustal deformation along the El Salvador Fault Zone from ZFESNet GPS network. Tectonophysics 670, 66–81.

Stein, R.S., 1999. The role of stress transfer in earthquake occurrence. Nature 402, 605–609.

Suárez, G., Muñoz, A., Farraz, I., Talavera, E., Tenorio, V., Novelo-Casanova, D., Sánchez, A., 2016. The 10 April 2014 Nicaraguan crustal earthquake: evidence of complex deformation of the central American volcanic arc. Pure Appl. Geophys. 173, 3305–3315.

Vallance, J., Houghton, B., 2004. The A.D. 260 Eruption at Lake Ilopango. El Salvador. A Complex Explosive Eruption through a Caldera Lake. National Science Foundation, Research Proposal, 1998.

Van Wyk de Vries, B., Merle, O., 1998. Extension induced by volcanic loading in regional strike-slip zones. Geology 26, 983–986.

White, R., 1991. Tectonic implications of upper-crustal seismicity in Central America. In: B, D., Engdahl, E.R., Zoback, M.D., Blackwell, D. (Eds.), Neotectonics of North America: Slemmons. Geological Society of America, Boulder, Colorado, pp. 323–338.

White, R., Harlow, D., 1993. Destructive upper-crustal earthquakes of Central America since 1900. Bull. Seismol. Soc. Am. 83, 1115–1142.

White, R., Alvarez, S., Harlow, D., 1987. The San Salvador earthquake of October 10, 1986; Seismological aspects and recent local seismicity. Earthq. Spectra 3, 419–434.

White, R., Ligorria, J., Cifuentes, I., 2004. Seismic history of the Middle America subduction zone along El Salvador, Guatemala, and Chiapas, Mexico: 1526-2000. In: Rose, W.I., Bommer, J.J.L., Lopez, D., Carr, M.J., Major, J.J., Soc, Geol, Pap, Am Spec (Eds.), Natural Hazards in El Salvador, vol. 375. The Geological Society of America, Boulder, pp. 379–396.

Yuan, A., Harlow, D., McNutt, S., 1984. Seismicity and the eruptive activity at fuego volcano, Guatemala, february 1975-january 1977. J. Volcanol. Geoth. Res. 21, 277–296.